Influence of particle dynamics on the instability for pattern formation in shallow pulsed beds

Lilian de Martín*
Department of Chemistry and Chemical Engineering, Chalmers University of Technology, 41296 Gothenburg, Sweden

(Received 13 June 2018; published 19 December 2018)

A granular layer can form standing-wave patterns, such as squares, stripes, and hexagons, when it is fluidized with a pulsed gas flow. These patterns resemble the well-known patterns formed in vertically vibrated granular layers, but are governed by different dimensionless numbers. Recent research [de Martín *et al.*, Phys. Rev. Fluids **3**, 034303 (2018)] reveals that the onset to pattern formation in shallow pulsed beds can be understood in terms of the dimensionless number $\Gamma_p = u_a/u_t\bar{\phi}$, where u_a is the amplitude of the gas velocity, u_t is the terminal velocity of the particles, and $\bar{\phi}$ is the average solids volume fraction. In contrast, pattern formation in vertically vibrated granular layers *in vacuo* is governed by the dimensionless number $\Gamma_v = 4\pi^2 f^2 d/g$, where f and d are the frequency and displacement of the vibrated plate, respectively, and g is the gravitational acceleration. In addition, the threshold for pattern formation in pulsed beds exhibits a strong dependence with the frequency of the excitation that is not observed in the threshold for pattern formation in vibrated systems. This work explores the origin of these differences by simulating the dynamics of a one-dimensional pulsed array of particles. Simulations reproduce well the experimental stability curves, and reveal that the criterion for instability in shallow pulsed and vibrated systems is actually the same; the layer flight time must be equal to $1/f$. In pulsed beds, this criterion is determined by the traveling time of the kinematic wave that forms in each flow pulse. These results provide a theoretical basis to the recent experimental observations and highlights commonalities between the mechanisms behind pattern formation in thin vibrated granular layers and shallow pulsed fluidized beds.

DOI: 10.1103/PhysRevFluids.3.124304

I. INTRODUCTION

Pulsed fluidization is a special type of fluidized-bed operation in which part of or all the fluid flow oscillates in time instead of being constant. Pulsation has various effects on the bed dynamics and has been used since the 1960 s as a method to improve the performance of gas-solid fluidized beds. Examples include the decrease of bubble size, control of agglomerate formation, or enhanced heat transfer [1]. However, the mechanisms behind these effects remain unclear and an overall picture of pulsed fluidization is missing. In particular, understanding how pulsed flow frequencies and particle characteristics interact in a pulsed bed has been recently highlighted as one of the main research questions in the field [1].

A distinct effect that pulsation can induce on a fluidized bed is the formation of periodic flow patterns. This phenomenon was observed two decades ago by Cheng *et al.* [2], who reported the formation of regular arrays of equidistant bubbles in a quasi-two-dimensional (quasi-2D) bed when

*lilian.de.martin@chalmers.se

it was fluidized with a square wave flow. In 3D geometries, this dynamical structuring visually manifests itself by the formation of striped, square, and hexagonal standing waves on the surface of the bed [3,4]. The patterns are subharmonic, meaning that they are shifted by half a wavelength every pulse and the exact configuration is repeated after two pulses. In very shallow beds (a few millimeters deep), the dense phase remains homogeneous and bubbleless and particles oscillate coherently. If the bed height is increased, bubbles gradually form in alternating positions that match the pattern antinodes, resulting in triangular bubble tessellations in quasi-2D geometries [5].

The rheology of patterned pulsed beds in the *shallow limit*, that is, the lowest bed height able to form dynamical mesostructures, has interesting properties. Standing-wave patterns in very shallow pulsed beds are the precursor of the bubble patterns that would form if the bed height were increased. The dense phase oscillates, but remains nearly homogeneous. Because bubbles do not form, the entire volume of gas percolates the dense phase, contributing to the expansion and minimizing interparticle friction. Simulations with discrete-element methods (DEM) and two-fluid models (TFM) show that the bed operates close to the viscous limit if the gas velocity is sufficiently high. Both DEM without interparticle friction and TFM with a viscous tensor are able to simulate standing-wave patterns in very shallow beds, showing that interparticle friction is not a necessary condition for pattern formation. This is consistent with the well-known fact that particle-phase inertia and drag are the only requirements to induce instability [6]. The drag, which is a function of the solids volume fraction, yields a kinematic wave with a speed that differs from the mean velocity of the particles. This voidage wave induces a time-dependent drag force on the particles, which is overshot by particle inertia [7].

If the bed height is increased, the nonlinear mechanisms that expel the particles from the antinodes of the waves become active, leading to bubble formation. A fraction of the gas bypasses the dense phase, increasing the solids volume fraction. Interparticle friction and chain forces become important and the rheology transits to the plastic limit, as shown by DEM and TFM simulations [5,8]. Reproducing computationally regular bubble patterns in deep beds therefore requires one to properly capture granular mechanics in the vicinity of the plastic regime. Four attempts to reproduce regular bubble patterns in quasi-2D pulsed beds using DEM have been reported [5,9–11] and only the simulations conducted by Wu *et al.* [5] have successfully captured the clear alternating bubble formation observed in the experiments. Two attempts to reproduce these patterns with TFM have been reported [8,12] and none of them have captured the experimentally witnessed triangular bubble tessellations. This highlights the difficulty of reproducing the mechanisms of force transition for very dense gas-solid flows. This is not properly done by current two-fluid models and has been proven challenging even for Lagrangian approaches [9–11].

Despite the advancements at the computational front, the fundamental physics and specifics of this phenomenon remain unclear. Particularly interesting aspects are the similarities and differences between pattern formation in shallow pulsed beds and the well-known standing-wave patterns formed on the surface of vertically vibrated thin granular layers [13,14]. Li *et al.* [3] showed that patterns in pulsed beds follow a dispersion relationship similar to the patterns formed in vertically vibrated granular layers. A detailed experimental study on the driving parameters governing the instability in shallow pulsed beds of Geldart B (sandlike) particles has been reported recently by de Martín *et al.* [4]. These authors observed that the threshold for pattern formation exhibits universal scaling and can be understood in terms of the dimensionless numbers $\Gamma_p = u_{a,c}/u_t\bar{\phi}$ and f/f_n (Fig. 1), where $u_{a,c}$ is the minimum amplitude of the gas velocity that triggers the patterns, u_t is the terminal velocity of the particles, $\bar{\phi}$ is the average solids volume fraction, f is the frequency of the oscillating gas velocity, and f_n is the natural frequency of the bed. It was observed that Γ_p exhibits a strong dependence of the forcing frequency f and layer height. In contrast, pattern formation in vertically vibrated granular layers is governed by the driving parameter $\Gamma_v = 4\pi^2 f^2 d/g$, where d is the displacement of the vibrating plate and g is the gravitational acceleration. Patterns form for $\Gamma_{v,c} \sim 2.5$–3 and exhibit a weak dependence on the forcing frequency and layer height [13,15]. It is clear that these differences arise from the different nature of the excitations, but the reasons behind the definition of Γ_p, the scaling with f_n, and the strong dependence of Γ_p with f/f_n (Fig. 1) are

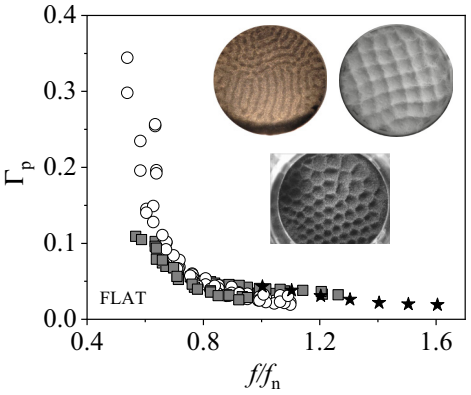

FIG. 1. Experimental stability curve for pattern formation in shallow pulsed beds, adapted from [4]: ○, glass 237; ■, glass 130; and ★, polystyrene. The parameters are $\Gamma_p = u_{a,c}/u_t\bar{\phi}$ and $f_n = \frac{1}{\pi}\sqrt{\frac{g}{h}}$.

open to dispute. It has been speculated that Γ_p could be related to the formation of kinematic waves in the bed, which are known to be instability drivers and whose velocity is determined by u_t and $\bar{\phi}$ [4].

In vibrated granular layers, the forcing comes from the vibrating plate and is only exerted when the layer is in contact with its surface. In their pioneer work, Melo *et al.* [13] suggested that standing-wave patterns appear when the layer flight time t_{fl} becomes equal to $1/f$. An estimation of t_{fl} was obtained by modeling the 1D motion of a single inelastic ball colliding with an oscillating surface, also known as the bouncing ball model. The theoretical threshold that provided the condition $t_{\mathrm{fl}} = 1/f$ was $\Gamma_{v,c} = 3.30$, in agreement with the experimental results. A more elaborate study by the same authors [14] revealed that the instabilities leading to the different patterns are governed by two dimensionless parameters: the layer free-flight time $\tau = f t_{\mathrm{fl}}$ and the acceleration of the granular layer relative to the plate during the time of collision $\gamma = u_c/g t_{\mathrm{fl}}$, where $u_c \propto 1/f$ is the relative collision velocity between the plate and the layer. It was observed that γ is nearly independent of f, which explains the weak dependence of Γ_v with the forcing frequency for pattern formation in vibrated systems. These authors also confirmed that the transition from a flat state to standing-wave patterns occurs when $\tau \sim 1$, especially at low values of f.

In pulsed beds, the forcing comes from the drag force exerted by the percolating pulsed flow, so the excitation is applied over the entire pulsation cycle and is strongly coupled to the bed dynamics through the bed expansion. The determination of t_{fl} and γ in pulsed beds is more challenging than in vibrated systems. In shallow beds, t_{fl} cannot be experimentally determined by accelerometers or pressure measurements and the visual determination is impeded by the flanges that connect the wind box and freeboard of a typical setup [4]. A theoretical estimation of these parameters from a model based on a single ball, similar to the approach used by Melo *et al.* [13,14], is not suited either because such a model would not capture the interplay between the drag force and the bed expansion.

The goal of this contribution is to understand the main qualitative features of the experimental stability curves shown in Fig. 1 and how they connect with fluidization dynamics. Since instabilities in very shallow beds are generated by particle inertia and drag, one of the simplest approaches that can capture this interplay is the particle array model (PAM) originally proposed by Broadhurst [16]. Particle array model simulations reproduce the main qualitative features of the stability curves and reveal that the condition for pattern formation in pulsed fluidized beds and vertically vibrated granular layers is actually the same: the layer flight time must be equal to $1/f$. In pulsed beds, the flight time refers to the timescale characterizing the expansion and contraction cycles. This time is determined by the velocity of the kinematic wave that forms by a change in the gas velocity. The differences in the definition of the driving parameters and shape of the stability curve between

pulsed beds and vibrated granular layers come from the different nature of the excitation forces. In pulsed fluidized beds, the divergence in Γ_p at low frequencies results from the dependence of the excitation, i.e., drag force, with the bed expansion.

This study provides a theoretical basis to the experimental observations recently presented in [4] and confirms that the threshold for pattern formation in shallow pulsed beds is not determined by the frictional properties of the particles. It sheds light on the interplay between flow frequencies and particle characteristics in conventional pulsed fluidized beds. This can be used, for instance, to understand the effect of the type of pulsation, e.g., square vs sinusoidal on the fluidization dynamics. Although industrial fluidized beds are deeper than the beds investigated in this work, the insights obtained from the study of very shallow beds can be used as a basis to understand more complex scenarios.

II. PARTICLE ARRAY MODEL

PAM represents a vertical array of fluidized particles whose motion is constrained to the vertical direction. It was originally proposed by Broadhurst [16] to understand the coherent and regular particle oscillations that are observed in very shallow gas-fluidized beds. Verloop and Heertjes [17] postulated that these oscillations are necessary precursors of bubble formation in deep beds and are dominated by particle inertia. This hypothesis is consistent with the well-known fact that a sufficient condition for instability in gas-solid flows is the interplay between particle inertia and drag [6]. PAM is one of the most simplified models accounting for this interplay, which explains its success in capturing a remarkable number of fluid mechanical aspects related to bubble formation, such as the change in particle behavior from oscillating to damped that is associated with the transition from bubbling to particulate fluidization [16]. In PAM, particle oscillations create local areas with a concentration of particles lower than the average. The gas flows preferentially through these areas, which grow in size to form bubbles if the bed is sufficiently deep. If particle oscillations do not occur due to the properties of the gas and the solid, the void fraction around each particle remains uniform and the fluid does not migrate to localized sites. Schouten and van den Bleek [18] showed that the dynamics reproduced by PAM presents chaotic features similar to those found in fluidized beds. Sierra *et al.* [19] concluded that, despite the severe simplifications, PAM is able to reproduce the temporal dynamics of deep fluidized beds.

Standing-wave patterns in shallow pulsed beds are a regular manifestation of the same instability that generates bubbles in deep beds. This phenomenon is known as phase locking in the field of nonlinear sciences and chaos control and occurs when the phase of a chaotic dynamics is synchronized with an external forcing. To induce locking, the timescale of the forcing must be close to a characteristic timescale of the system, such as the natural period. Once locked, the dynamics is no longer chaotic, but operates in discrete states of the phase space. PAM not only captures aspects of bubble formation, but also is able to reproduce the phase locking that occurs when a bed is fluidized with a pulsating flow. Van de Klundert [20] showed that when an array of Geldart B particles is fluidized with a constant gas flow, PAM reproduces a chaotic movement of the particles analogous to the disorganized dynamics characterizing conventional fluidized beds. However, if particles are fluidized with a square wave gas velocity, particle motion becomes regular under certain conditions, analogously to the structured dynamics observed in patterned pulsed beds.

In this work PAM is used to reproduce the main qualitative features of the stability curve shown in Fig. 1 and unravel what particular criterion is satisfied when the dynamics transits from chaotic to ordered. It is important to clarify that PAM is an abstraction used here to gain insight into the phenomenon of dynamical locking that leads to pattern formation. Models with similar level of simplification are the bouncing ball model used by Melo *et al.* [13,14], used to explain the stability chart in pattern formation in vertically vibrated granular layers, or the second-order oscillator used in the fluidization field to explain the natural frequency of the bed [21]. These models are aimed not at describing granular physics at a quantitative level, but to target particular dynamical aspects.

In PAM, the only two forces acting over each particle i are its weight and the local drag force exerted by the fluid. A force balance for each particle reads

$$\rho_p \frac{\pi d_p^3}{6} \frac{d^2 h_i}{dt^2} = \frac{\pi d_p^2}{4} \frac{\rho_f v_i^2}{2} C_{d,i} - \frac{\pi d_p^3}{6} (\rho_p - \rho_f) g, \tag{1}$$

where ρ_p and ρ_f are the particle and fluid density, respectively, d_p is the particle size, v_i is the relative motion between particle i and the gas, and h_i is the height of particle i. The drag coefficient $C_{d,i}$ is calculated with the Ergun equation

$$C_{d,i} = \frac{200(1-\epsilon_i)}{\epsilon_i^3 \mathrm{Re}} + \frac{2.33}{\epsilon_i^3}, \tag{2}$$

where ϵ_i is the voidage for particle i. The Ergun equation loses validity for Reynolds numbers larger than $\mathrm{Re} \sim 500$ [22]. However, the largest Reynolds number in this work is $\mathrm{Re} \sim 50$, obtained for 1-mm particles at a maximum superficial gas velocity of $u_0 = 0.75$ m/s.

The relative motion between the particle and gas is $v_i = \frac{u_0}{\epsilon_i} - v_{p,i}$, where $v_{p,i} = \frac{dh_i}{dt}$ is the velocity of particle i and u_0 is the superficial gas velocity, which is assumed to vary sinusoidally [4] $u_0 = \bar{u} + u_a \sin(2\pi f t)$, with $\bar{u} = u_{\min} + u_a$. Here $u_{\min} = 1.05 u_{\mathrm{MF}}$, a condition that leads to the formation of stable and regular patterns in the experiments [4,23]. It is assumed that u_0 changes instantaneously in the whole domain, a reasonable assumption since the simulated bed heights are on the order of millimeters. Equation (1) is made dimensionless by defining the variables $L_i = \frac{h_i}{d_p}$, $\theta = t \frac{\bar{u}}{d_p}$, and $\beta = \frac{\rho_p}{\rho_f}$, that is,

$$\frac{d^2 L_i}{d\theta^2} = \frac{1}{\beta \bar{u}^2} \left(\frac{u_0}{\epsilon_i} - \bar{u} \frac{dL_i}{d\theta} \right)^2 \left[\frac{150}{\mathrm{Re}} \frac{1-\epsilon_i}{\epsilon_i} + \frac{1.75}{\epsilon_i} \right] - \frac{1}{\beta} \frac{\mathrm{Ar}}{\overline{\mathrm{Re}}^2}, \tag{3}$$

where the Archimedes number $\mathrm{Ar} \equiv \frac{(\rho_p - \rho_f)\rho_f g d_p^3}{\mu^2}$, $\overline{\mathrm{Re}} \equiv \frac{\rho_f \bar{u} d_p}{\mu}$, and $\mathrm{Re} \equiv \frac{\rho_f u_0 d_p}{\mu}$. For a constant gas velocity $u_0 = \bar{u}$ and Eq. (3) is the same as the equation used in [16,18]. Note that the Reynolds number Re, used in the definition of the drag coefficient, does not take into account particle motion. Fluidizing gas is assumed to be air at room conditions, so $\rho_f = 1.2\ \mathrm{kg/m^3}$ and $\mu = 1.8 \times 10^{-5}$ Pa s.

A critical aspect of PAM is the relationship between interparticle distance L_i and local voidage ϵ_i. Broadhurst [16] provided an expression for ϵ_i based on the similarity between a particle at a specific height and the rotameter bob in a gas flow. This method requires defining the angle of the semidivergent cone, so Schouten and van den Bleek [18] provided a simpler expression in which ϵ_i is calculated from the distance between a particle and its lower neighbor, $\phi_i = \phi_0/(L_i - L_{i-1})$, where $\phi_0 = 1 - \epsilon_0$ is the initial solids volume fraction. This expression was tested in this work, but the simulations did not reproduce the trends observed in the experiments, especially towards low values of the flow frequency, where the stability curve bent instead of smoothly increased.

Here, a different function is proposed. It assumes that the array of particles is immersed in a 3D bed, so the local volume fraction depends not only on the vertical distance to the neighboring particles, but also on the horizontal distance to the hypothetical (ghost) neighbors. Given the random nature of particle motion, it is assumed that the average interparticle distance in the three directions is the same. This is better illustrated considering the cubic lattice shown in Fig. 2. If the distance between particles is l, the solids volume fraction in the cubic lattice is $\phi \propto (\frac{d_p}{l})^3$, so $\phi \propto L^{-3}$. Assuming that L is equal to the average distance between a particle i and its neighbors $i-1$ and $i+1$ in the 1D array, so $L = (L_{i+1} - L_{i-1})/2$, and imposing the correct limit ϕ_0 at $L = 1$ gives

$$\phi_i = \phi_{i,0} \left(\frac{2}{L_{i+1} - L_{i-1}} \right)^3 \quad \text{for particles } i = 1, \ldots, N-1, \tag{4}$$

where $\phi_{i,0} = 0.58$, experimentally determined by pouring a known mass of particles in a graduated cylinder. This value slightly varies across particles, but for the sake of simplicity it is assumed the

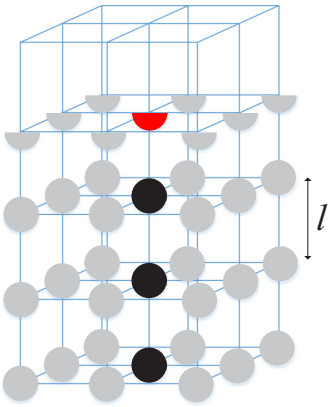

FIG. 2. Scheme to estimate the local solids volume fraction ϕ_i from the interparticle distance. Black particles represent the array of particles simulated with PAM. The red particle represents the top particle. Gray particles represent ghost particles included in the calculation of ϕ_i.

same for all. Since the top particle does not have upper neighbors, l is calculated from the distance to the lower neighbor

$$\phi_N = \phi_{N,0}\left(\frac{1}{L_N - L_{N-1}}\right)^3 \quad \text{for particle } i = N, \tag{5}$$

whereas the initial solids volume fraction is calculated as $\phi_{N,0} = \phi_{i,0}/2$ (Fig. 2).

Particle height is evaluated taking as reference the bottom of each particle, so the distributor is treated as a particle at a fixed position $L_0 = -1$. Particle collisions will be handled similarly to Schouten and van den Bleek [18]. The velocity component w_i after collision for two particles with equal masses is derived as

$$w_1 = u_1\frac{1-\mathcal{C}}{2} + u_2\frac{1+\mathcal{C}}{2}, \quad w_2 = u_1\frac{1+\mathcal{C}}{2} + u_2\frac{1-\mathcal{C}}{2}, \tag{6}$$

where u_i is the particle velocity before impact and $\mathcal{C}$ is the coefficient of restitution. In this work, $\mathcal{C} = 0.8$ for all particles, corresponding to the value for glass [18]. The time step is $\theta = 2\times10^{-4}$, selected by means of a sensitivity analysis.

III. RESULTS AND DISCUSSION

The properties of the simulated particles are displayed in Table I. Glass 130, glass 237, and polystyrene 600 are the Geldart B particles represented in Fig. 1. The simulated array heights for these solids also correspond to the bed heights investigated in [4]. D1000 and A130 particles belong to the Geldart D and A classifications [24], respectively, for which pattern formation has not been observed experimentally in a fluidized bed. The minimum fluidization velocity u_{MF} reported in Table I corresponds to the values obtained with PAM, which are somewhat different from the experimental values reported in [4].

The minimum amplitude of the oscillating gas velocity that makes the array of particles transit from a chaotic to a regular behavior, $u_{a,c}$, is taken as the threshold for locking conditions. This condition can be identified by plotting the position of the top particle L as a function of its velocity $dL/d\theta$ [18]. A locked phase can be recognized when the trajectories for the top particle overlap in a single orbit without any internal loop, similarly to the loop obtained from pressure fluctuation measurements obtained in a structured bed [25]. An example of the transition from chaotic to ordered dynamics for an array of glass 237 particles is illustrated in Fig. 3.

TABLE I. Particles and conditions simulated. For all cases $\mathcal{C} = 0.8$, $\epsilon_0 = 0.42$, and $u_{\min} = 1.05 u_{\mathrm{MF}}$, where u_{MF} is the minimum fluidization velocity.

Name	d_p (μm)	ρ_p (kg/m^3)	u_{MF} (m/s)	u_t (m/s)	Geldart	N
glass 130	130	2500	0.020	0.80	B	23, 30
glass 237	237	2500	0.064	1.74	B	13, 17, 21, 30
polystyrene 600	600	1040	0.154	2.49	B	17, 25
D1000	1000	2000	0.539	11.13	D	15
A130	130	1300	0.010	0.48	A	23

No locking conditions were found for Geldart A particles, which is consistent with the fact that no patterns have ever been observed for this powder. This has been attributed to the relatively large stability of the dense gas-solid suspensions of Geldart A particles, which can maintain a homogeneous state over a range of conditions broader than those for Geltart B and D powders [23]. In contrast, locking conditions were identified for Geldart D particles although no experimental patterns have been observed for this powder. Regelink [23] suggests that this could be due to experimental limitations, since Geldart D particles might require a very wide setup to form patterns due to the large bubble size characterizing their fluidization. The work of de Martín *et al.* [4] suggests that, if pattern formation in Geldart B and D particles is governed by the same principles, the lack of experimental patterns for Geldart D particles might be attributed to the large amplitude of the gas velocity required to induce them, difficult to reach with conventional laboratory-scale flow systems. Particle array model simulations confirm that the lack of experimental patterns for Geldart D particles is due to experimental limitations and not fundamental reasons. It is worth mentioning that the sharpness of the transition from chaotic to ordered dynamics depends on the type of solid. The heavier particles in glass 237, polysterene 600, and D1000 exhibit an abrupt transition when the amplitude of the gas velocity is increased, whereas the transition for glass 130 is smoother.

The threshold for locking dynamics for the particles displayed in Table I is shown in Fig. 4. The driving parameters are defined as in [4], where the natural frequency is calculated with Baskakov's model [21] $f_n = \frac{1}{\pi}\sqrt{\frac{g}{h}}$, where h is the bed height. The average solids volume fraction is estimated as $\bar{\phi} = \frac{1}{N}\sum_{i=1}^{N}\phi_i$. It is possible to observe that, despite the severe simplifications, PAM reproduces the main qualitative features of the experimental results shown in Fig. 2, confirming that the instability for pattern formation in shallow fluidized beds can be understood in terms of

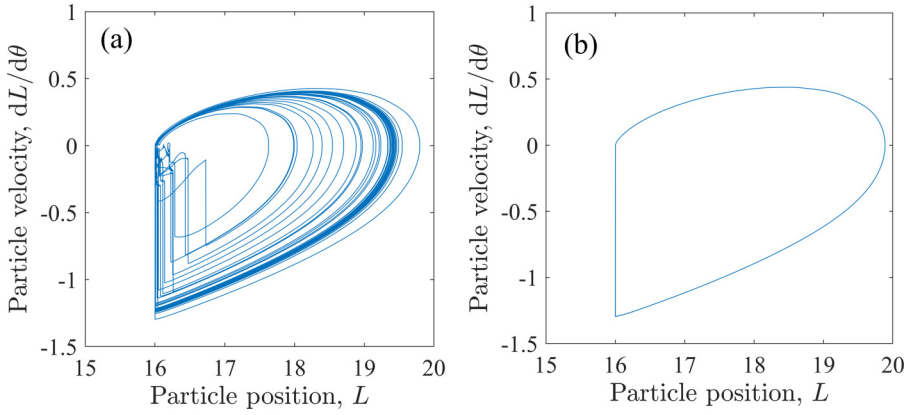

FIG. 3. Trajectories for the top particle between $t = 3$ and $t = 6$ s in an array of glass 237. A small increase in the amplitude of the oscillating gas velocity induces an abrupt change in the particle dynamics, from (a) disordered, $u_a/u_{\mathrm{MF}} = 0.34$, to (b) ordered, $u_a/u_{\mathrm{MF}} = 0.37$. The parameters are $N = 17$ and $f = 15$ Hz.

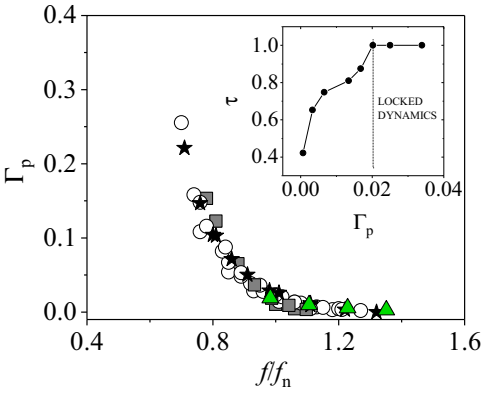

FIG. 4. Simulated stability curve for pattern formation in shallow pulsed beds, with the same conditions as for Fig. 1: ○, glass 237; ■, glass 130; ★, polystyrene; and ▲, D1000. The inset shows the evolution of τ with Γ_p for glass 237, with $N = 21$ and $f = 14$ Hz.

the dimensionless numbers $\Gamma_p = u_{a,c}/u_t\bar{\phi}$ and f/f_n. These results support the hypothesis that the onset to the instability emerges from the interplay between the drag and bulk dynamics, with no significant influence of interparticle friction [4]. Looking at the situation as a whole, these results are consistent with the well-known fact that, in a fluidized bed, particle-phase inertia and drag are the only requirements to induce the instability that leads to the formation of flow mesostructures, such as bubbles. The drag, which is a function of the solids fraction ϕ, yields a kinematic wave with a speed that differs from the mean velocity of the particles. This voidage wave induces a time-dependent drag force on the particles, which is overshot by particle inertia [7].

An interesting difference between simulated and experimental results is the behavior of the stability curve for large values of f. In the experiments, the threshold for pattern formation tends asymptotically to $\Gamma_p \sim 0.03$ for large frequencies, whereas in the simulations, it tends to $\Gamma_p \sim 0$. If the experimental results are not affected by artifacts, this means that there is a factor that suppresses the instability for pattern formation in the experiments but not in the simulations. Interparticle friction has been hypothesized in the literature as one of the factors that might suppress the instability for bubble formation [26] and could be a reason for this mismatch between the experimental and simulated results. An additional reason could be related to the 1D nature of the model and its implications in the concepts of granular temperature and viscosity. In a real 3D bed, particle motion has a random component in three directions, which induces random lateral forces. To induce collective behavior and phase locking, the forcing must overcome the incoherent motion of the particles, resulting in a minimum threshold to induce patterns. This incoherent particle motion is not present in an array of particles confined to one dimension. In other words, a reason for the mismatch could be that PAM does not capture the viscosity that would dampen the formation of standing-wave patterns. In fact, the threshold for pattern formation in inviscid liquids (Faraday waves) tends to zero. An additional force not included in PAM that could have an effect on the results is the Boussinesq-Basset force. This force is believed to be negligible in conventional gas-solid fluidization due to the random motion of the particles and their low accelerations. However, the flow in patterned beds is pulsed and particles are subjected to significant accelerations and decelerations and exhibit coherent motion. If the Boussinesq-Basset force delays the motion of the granular layer with respect to the gas flow, resulting in a lower bed expansion, the criterion $\tau = 1$ might be obtained for values of Γ_p larger than those obtained in the absence of the force.

PAM was originally proposed to explain particle dynamics in very shallow beds, in which bubble formation is hindered. It is therefore only applicable to arrays with a small number of particles N. In this sense, it is observed that the scaling shown in Fig. 4 only holds for $N \lesssim 25$–35, depending on the particle properties. Larger values of N progressively shift Γ_p towards lower frequencies.

An illustrative example of the evolution of $\tau = f t_{\mathrm{ft}}$ with Γ_p is shown in the inset of Fig. 4. Here the term t_{ft} is equivalent to the flight time used in the studies of pattern formation in vertically vibrated layers, but is defined differently. In vibrated systems, t_{ft} refers to the time span where the granular layer is not in contact with the excitation force, i.e., the oscillating plate. In fluidized beds, the term flight time is less adequate because particles are suspended at all times and the contact between the layer and the excitation is continuous, instead of intermittent. However, both systems can be reconciled if one assumes that the flight time characterizes the timescale of the oscillations of the granular layer. In this case, the flight time of a pulsed fluidized bed can be approximated as the average time between consecutive oscillations of the bed expansion. By using this definition of t_{ft}, it is observed that τ increases with Γ_p until a value $\tau = 1$ is reached (Fig. 4 inset), a condition that triggers the onset to locking conditions in the simulations. Once the dynamics is locked, τ remains constant over further increments in Γ_p. This behavior is equivalent to the variation of τ with Γ_v that Melo *et al.* [13,14] theoretically estimated from the bouncing ball model when studying pattern formation in vertically vibrated granular layers. The bouncing ball model predicts an increment of τ with Γ_v until $\tau = 1$ is reached at $\Gamma_{v,c} = 3.30$, a value that approximates well the experimental threshold for pattern formation, especially at low frequencies. Once the condition $\tau = 1$ is reached, a further increment in Γ_v no longer results in an increment in τ, similarly to the trend shown in the inset of Fig. 4. These results suggest that pattern formation in vibrated granular layers and pulsed fluidized bed form for periodic excitations that satisfy the condition $\tau \sim 1$ in both cases. This condition creates an interaction between subsequent rising and falling momentum fluxes that is associated with the formation of standing-wave patterns [13].

After this insight, the interpretation of the main features of the stability curves shown in Figs. 1 and 4 is straightforward. For large frequencies of the gas velocity, the condition $\tau \sim 1$ is satisfied with short expansion and compression cycles. Short cycles are linked to small bed expansions, which are achieved with a small amplitude of the gas pulses. When the frequency of the gas velocity is decreased, longer expansion and compression cycles are required to satisfy $\tau \sim 1$. Longer cycles are linked to larger bed expansions, which are achieved through a larger amplitude of the gas velocity. However, the larger the bed expansion is, the lower the drag coefficient $C_{d,i}$ becomes [Eq. (2)] and the larger the amplitude of the gas velocity must be to further increase the bed expansion. This interplay between the drag and the bed expansion is one of the reasons that causes the sharp increase of Γ_p at low frequencies. In vibrated systems, there is no such strong coupling between the excitation and the layer dynamics and t_{ft} mostly depends on the frequency and amplitude of the oscillating plate if the experiments are conducted *in vacuo*.

The condition $\tau = 1$ also explains why the experimental threshold for pattern formation in pulsed beds is lower when the shape of the oscillating gas velocity is square instead of sinusoidal as observed in the experiment. The same increase in the gas velocity will generate a larger bed expansion if the change is applied sharply instead of smoothly. Thus, for the same amplitude of the gas velocity, t_{ft} is larger for a square wave pulse, which implies lower thresholds to achieve $\tau = 1$ for the same cycle frequency of the gas velocity. These results note the importance of controlling the shape of the oscillating gas velocity when applying pulsed flows to intensify fluidization. Pulsation is often realized with on-off valves, which are intended to generate quasisquare wave pulses. However, in the absence of a feedback control loop, the actual shape of the oscillating gas velocity will be determined by the design of the setup and flow system, and flow properties due to nonlinear hydrodynamical effects and pressure buildup. This variation in the wave shape could be a reason for the apparent inconsistency in the results across some pulsation studies [1]. Furthermore, the concept of *frequency* cannot be unequivocally defined when the gas velocity deviates from a sinusoid [27].

If the instability behind pattern formation occurs by the interaction of rising and falling momentums generated by the coupling between the oscillating gas velocity and the expansion and compression cycles, the role of the kinematic wave speculated by de Martín *et al.* [4] becomes apparent. These authors suggested that the origin of the terms $u_t\bar{\phi}$ in the definition of Γ_p could be related to the formation of kinematic waves, which are known to be instability drivers and

whose velocity u_k is determined by both u_t and ϕ. However, the mechanistic understanding of how the kinematic wave, also known as a voidage wave, could engage in the instability for pattern formation was unclear. The condition $\tau = 1$ sheds light on this question because in a fluidized bed, the timescale characterizing the expansion and compression cycles generated by an abrupt change in the gas velocity is determined by the speed of the kinematic wave u_k and bed height h [28]. When a homogeneous bed is subjected to a step change in the fluidizing gas velocity, a kinematic wave originates in the distributor and rises through the bed. Simultaneously, the bed height increases, if the step is positive, or decreases, if the step is negative. The bed reaches a new equilibrium when the wave reaches the final position of the surface. This phenomenon is poorly understood and a mathematical description is only available when the flow step is very small and sharp. In any case, the time of the expansion and compression cycles is associated with the traveling time of the kinematic wave $t_k = f(h/u_k)$, in agreement with the strong dependence of the threshold for pattern formation with the bed height in pulsed beds.

IV. CONCLUSION

The formation of standing-wave patterns in vertically vibrated granular layers and in pulsed fluidized beds share a similar instability criterion. In both systems, patterns appear when the timescale of the forcing is equal to the timescale of the oscillations of the layer, creating an interaction between subsequent rising and falling momentum fluxes. However, due to the different nature of the excitations, this criterion is governed by different dimensionless numbers and is revealed through different stability curves. In vertically vibrated systems *in vacuo*, the timescale of the layer motion is mainly governed by the amplitude and frequency of the vibrating plate, and gravity. In pulsed beds, the timescale of the expansion and contraction cycles is governed by the traveling time of the kinematic wave that forms in each cycle.

This insight is a step towards understanding the relationship between flow and particle properties in pulsed fluidization and can be used, for instance, to unravel the effect of the type of pulsation, e.g., square vs sinusoidal, on the fluidization dynamics. Getting a functional form for the dependence between Γ_p and f is the object of existing research. However, further insight into the formation and propagation of kinematic waves under continuously varying gas velocities is needed for this purpose.

ACKNOWLEDGMENT

The author would like to thank Professor Anders Rasmuson and Masood Tamadondar for commenting on the manuscript.

[1] E. Ireland, K. Pitt, and R. Smith, A review of pulsed flow fluidization; the effects of intermittent gas flow on fluidised gas-flow bed behaviour, Powder Technol. **292**, 108 (2016).

[2] Y. Cheng, S. Kaart, C. M. van den Bleek, and M.-O. Coppens, in *Proceedings of the AIChE Annual Meeting*, edited by L. Glicksman (AIChE, Dallas, 1999), Vol. 31, pp. 312–319.

[3] J. Li, I. S. Aranson, W.-K. Kwok, and L. S. Tsimring, Periodic and Disordered Structures in a Modulated Gas-Driven Granular Layer, Phys. Rev. Lett. **90**, 134301 (2003).

[4] L. de Martín, C. Ottevanger, J. R. van Ommen, and M.-O. Coppens, Universal stability curve for pattern formation in pulsed gas-solid fluidized beds of sandlike particles, Phys. Rev. Fluids **3**, 034303 (2018).

[5] K. Wu, L. de Martín, and M.-O. Coppens, Pattern formation in pulsed gas-solid fluidized beds—The role of granular solid mechanics, Chem. Eng. J. **329**, 4 (2017).

[6] R. Jackson, in *The Dynamics of Fluidized Particles*, edited by R. Jackson (Cambridge University Press, Cambridge, 2000).

[7] D. L. Koch and A. Sangani, Particle pressure and marginal stability limits for a homogeneous monodisperse gas-fluidized bed: Kinetic theory and numerical simulations, J. Fluid Mech. **400**, 229 (1999).
[8] K. Wu, L. de Martín, L. Mazzei, and M.-O. Coppens, Pattern formation in fluidized beds as a tool for model validation: A two-fluid model based study, Powder Technol. **295**, 35 (2016).
[9] T. Kawaguchi, A. Miyoshi, T. Tanaka, and Y. Tsuji, Discrete particle analysis of 2D pulsating fluidized bed, in *Proceedings of the 4th International Conference on Multiphase Flow (ICMF-2001)* (New Orleans, USA, 2001), paper 838.
[10] X. S. Wang and M. J. Rhodes, Pulsed fluidization—A DEM study of a fascinating phenomenon, Powder Technol. **159**, 142 (2005).
[11] D. G. de Oliveira, O. O. Ayeni, C. L. Wu, K. Nandakumar, and J. B. Joshi, in *Proceedings of the Seventh International Conference on Discrete Element Methods*, edited by X. Li, Y. Feng, and G. Mustoe, Springer Proceedings in Physics Vol. 188 (Springer, Singapore, 2017), p. 619.
[12] A. Bakshi, C. Altantzis, A. Bershanska, A. K. Stark, and A. F. Ghoniem, On the limitations of 2D CFD for thin-rectangular fluidized bed simulations, Powder Technol. **332**, 114 (2018).
[13] F. Melo, P. B. Umbanhowar, and H. L. Swinney, Transition to Parametric Wave Patterns in a Vertically Oscillated Granular Layer, Phys. Rev. Lett. **72**, 172 (1994).
[14] F. Melo, P. B. Umbanhowar, and H. L. Swinney, Hexagons, Kinks, and Disorder in Oscillated Granular Layers, Phys. Rev. Lett. **75**, 3838 (1995).
[15] T. H. Metcalf, J. B. Knight, and H. M. Jaeger, Standing wave patterns in shallow beds of vibrated granular material, Physica A **236**, 202 (1997).
[16] T. E. Broadhurst, in *Encyclopedia of Fluid Mechanics* (Gulf, Houston, 1986), Vol. 4, Sec. I, Chap. 25, p. 781.
[17] J. Verloop and P. M. Heertjes, On the origin of bubbles in gas-fluidized beds, Chem. Eng. Sci **29**, 1101 (1974).
[18] J. C. Schouten and C. M. van den Bleek, Chaotic hydrodynamics of fluidization: Consequences for scaling and modeling of fluid bed reactors, AIChE Symp. Ser. **88**, 70 (1992).
[19] C. Sierra, L. Tadrist, and R. Ocelli, Local and global dynamics of shallow gas-fluidized beds, Phys. Fluids **18**, 043303 (2006).
[20] R. van de Klundert, Pattern formation in pulsated fluidized beds and vertically vibrated granular layers, M.Sc. thesis, TU Delft, 2001.
[21] A. P. Baskakov, V. G. Tuponogov, and N. F. Filippovsky, A study of pressure fluctuations in a bubbling fluidized bed, Powder Technol. **45**, 113 (1986).
[22] J. A. Tallmadge, Packed bed pressure drop-an extension to higher Reynolds numbers, AIChE J. **16**, 1092 (1970).
[23] M. Regelink, Formation of regular bubble patterns in periodically pulsed gas-solid fluidised beds, M.Sc. thesis, TU Delft, 2000.
[24] D. Geldart, Types of gas fluidization, Powder Technol. **7**, 285 (1973).
[25] D. V. Pence and D. E. Beasley, Chaos suppression in gas-solid fluidization, Chaos **8**, 514 (1998).
[26] S. Sundaresan, Instabilities in fluidized beds, Annu. Rev. Fluid Mech. **35**, 63 (2003).
[27] N. E. Huang, Z. Wu, S. R. Long, K. C. Arnold, X. Chen, and K. Blank, On instantaneous frequency, Adv. Adapt. Data Anal. **1**, 177 (2009).
[28] L. Gibilaro, *Fluidization-Dynamics* (Butterworth-Heinemann, Oxford, 2001).